

bradscholars

Aggregate interlock in lightweight concrete continuous deep beams

Item Type	Article
Authors	Yang, Keun-Hyeok;Ashour, Ashraf
Citation	Yang KH and Ashour AF (2011) Aggregate Interlock in Lightweight Concrete Continuous Deep Beams. Engineering Structures Journal, 33(1):136-145.
DOI	https://doi.org/10.1016/j.engstruct.2010.09.026
Rights	© 2011 Elsevier. Reproduced in accordance with the publisher's self-archiving policy.
Download date	2026-03-05 10:57:01
Link to Item	http://hdl.handle.net/10454/7562



The University of Bradford Institutional Repository

<http://bradscholars.brad.ac.uk>

This work is made available online in accordance with publisher policies. Please refer to the repository record for this item and our Policy Document available from the repository home page for further information.

To see the final version of this work please visit the publisher's website. Available access to the published online version may require a subscription.

Link to original published version: <http://dx.doi.org/10.1016/j.engstruct.2010.09.026>

Citation: Yang KH and Ashour AF (2011) Aggregate Interlock in Lightweight Concrete Continuous Deep Beams. *Engineering Structures Journal*, 33(1):136-145.

Copyright statement: © 2011 Elsevier. Reproduced in accordance with the publisher's self-archiving policy.



AGGREGATE INTERLOCK IN LIGHTWEIGHT CONCRETE

CONTINUOUS DEEP BEAMS

Keun-Hyeok Yang^a, Seol Lee^b, and Ashraf F. Ashour^c

^a *Corresponding author, Department of Architectural Engineering, Mokpo National University, Mokpo, Jeonnam, South Korea. Tel: 82 (0)61 450 2456; Fax: 82 (0)61 450 6454; E-mail: yangkh@mokpo.ac.kr*

^b *Department of Architectural Engineering, Mokpo National University, Mokpo, Jeonnam, South Korea.*

^c *EDT 1, School of Engineering, Design and Technology, University of Bradford, Bradford, BD7 1DP, UK.*

Biography: Keun-Hyeok Yang is an associate professor at Mokpo National University, South Korea. He received his MSc and PhD degrees from Chungang University, South Korea. He was a visiting research fellow at the University of Bradford, UK. His research interests include ductility, recycling, strengthening, plasticity, and shear of reinforced eco-friendly concrete structures.

Seol Lee is a doctoral student at Mokpo National University, South Korea. Her research interests include shear and plasticity of reinforced eco-friendly concrete structures.

Ashraf F. Ashour is the director of civil engineering at the University of Bradford, UK. He obtained his BSc and MSc degrees from Mansoura University, Egypt and his PhD from Cambridge University, UK. His research interests include shear, plasticity and optimization of reinforced concrete and masonry structures.

ABSTRACT

This paper presents the testing of 12 continuous beams made of all-lightweight, sand-lightweight and normal weight concrete having maximum aggregate sizes of 4, 8, 13 and 19 mm. All beams had the same geometrical dimensions and steel reinforcement. Load capacity of beams tested are compared with the predictions from strut-and-tie models recommended in ACI 318-08 and EC 2 provisions including the modification factor for lightweight concrete. Test results showed that the amount of load transferred to the intermediate support after the occurrence of the diagonal crack within the interior shear spans and load capacity increased with the increase of the maximum aggregate size, though the aggregate interlock contribution to load capacity in lightweight concrete deep beams was less than that in normal weight concrete deep beams. The lightweight concrete modification factor in EC2 is generally unconservative, while that in ACI318-08 is conservative for all-lightweight concrete but turns to be unconservative for sand-lightweight concrete with a maximum aggregate size above 13mm. It was also shown that the conservatism of the strut-and-tie models specified in ACI 318-08 and EC 2 decreased with the decrease of the maximum aggregate size, and was less in lightweight concrete deep beams than in normal weight concrete deep beams.

Keywords: lightweight concrete, continuous deep beam, aggregate size, modification factor, strut-and-tie model.

INTRODUCTION

Shear is transmitted in a cracked concrete slender beam without shear reinforcement in different ways including dowel action of main longitudinal reinforcement, aggregate interlock and shear in the uncracked concrete compression zone. However, deep beams can also transfer a large amount of applied loads through diagonal struts even after the occurrence of diagonal cracks [1-3]. Taylor [4] concluded that 50% of the applied shear force can be transferred by aggregate interlock in slender beams tested. Fenwick and Paulay [5] also pointed out that aggregate interlock contribution to the

shear capacity of beams without shear reinforcement would increase with the decrease of shear span-to-depth ratio due to the steeper angle of diagonal cracks. However, very few [6], if any, investigations on aggregate interlock in deep beams are available in the literature, though aggregate interlock can play a significant role in load transfer of concrete struts with diagonal cracks.

Aggregate interlock contribution to the shear capacity of beams is significantly dependent on the shape, size and strength of coarse aggregate as well as concrete compressive strength [6]. The regression analysis carried out by Bažant and Sun [7] revealed that the shear capacity of slender beams without shear reinforcement increases with the increase of the maximum aggregate size. On the other hand, it was observed [8] that the aggregate interlock capacity decreased in beams with a smoother failure surface owing to cracks penetrating through the coarse aggregate particles. As a result, the simplified modified compression field theory [9, 10] neglects the shear stresses transferred by aggregate interlock along cracks in beams having concrete strength above 70 MPa and lightweight concrete beams. However, there is no apparent evidence for the reduced effect of aggregate interlock on the shear capacity of lightweight concrete beams.

The load capacity of deep beams predicted by strut-and-tie models (STMs) is significantly dependent on the effective strength of concrete struts [11]. Most design codes [1, 2] propose a modification factor associated with the effective strength of concrete to account for the reduced friction properties of diagonal crack interfaces in lightweight concrete struts. A few comparative investigations [12, 13] explored the conservatism of STMs specified in code provisions for normal weight concrete deep beams, yet acceptable conclusions for lightweight concrete deep beams is very rare. In particular, the modification factor of the effective strength of lightweight concrete struts in deep beams is fundamentally based on shear test results of slender beams and material properties such as splitting tensile strength.

The principal aim of the present study is to evaluate the effect of aggregate size on the structural behavior of lightweight concrete continuous deep beams without shear reinforcement. The

distribution and width of diagonal cracks, redistribution of the applied load after the occurrence of diagonal cracks within the interior shear spans, and load capacity of beams tested are examined against the variation of aggregate size and concrete type. In addition, the conservatism of STMs specified in ACI 318-08 [1] and EC 2 [2] provisions including the modification factor for lightweight concrete is assessed for lightweight concrete continuous deep beams.

EXPERIMENTAL PROGRAMME

Test specimen details

Reinforced concrete deep beams are frequently constructed over several supports. The occurrence of inflection points and coexistence of high shear and high moment within interior shear spans of continuous deep beams have a considerable effect on crack propagation and aggregate interlock along diagonal cracks in concrete struts, and eventually a significant reduction of effective strength of concrete struts. Hence, the current testing programme covers twelve continuous concrete deep beam specimens having different aggregate size and concrete type, as given in Table 1. The maximum size of aggregate, d_a , varied from 4 mm to 19 mm in each concrete group; all-lightweight concrete (ALWC), sand-lightweight concrete (SLWC), and normal weight concrete (NWC) groups. The beam specimens with 4 mm maximum aggregate size resemble a mortar-like beam specimen without coarse aggregate.

All beams tested had the same geometrical dimensions and reinforcement as shown in Fig. 1. The section width, b_w , and overall depth, h , were 200 mm and 400 mm, respectively, and the shear span-to-overall depth ratio, a/h , was 0.54. Both longitudinal top and bottom reinforcement ratios were kept constant in all beams at 0.016. The longitudinal top and bottom reinforcing bars were continuous over the full length of the beam tested and welded to 160×100×10 mm end steel plates for anchorage purposes. No shear reinforcement was provided in the test zone between the centers of both end supports. The beam notation given in Table 1 identifies the type of concrete (“A” for all-

lightweight concrete, “S” for sand-lightweight concrete and “N” for normal weight concrete) and the maximum aggregate size, respectively. For example, A8 is an all-lightweight concrete continuous beam with aggregate size of 8mm.

Material properties

The physical properties of aggregates used in beam specimens are given in Table 2. Artificially expanded clay granules composed of quartz and calcium aluminum silicate as recorded from X-ray diffraction were used for structural lightweight aggregates. The lightweight aggregate features a spherical shape of a closed surface with a slightly rough texture. The core of lightweight aggregate particles has a uniformly fine and porous structure. Crushed andesite and natural sand of a maximum particle size of 4 mm were also used for normal weight coarse and fine aggregates, respectively.

The net area and yield strength of main longitudinal steel bars are 287 mm² and 508 MPa, respectively. The design compressive strength and initial slump of ready-mixed concrete were 30 MPa and 150 mm in all beam specimens. The mix proportions of each concrete determined from the preliminary laboratory tests are given in Table 1. Commercially available poly carboxylate-based superplasticizer was added in all concrete mixes but specimens S4 and N4 as both specimens met the target slump even without superplasticizer. For the ALWC mix series except specimen A4, 11.1% silica fume relative to the amount of cement was added to meet the designed compressive strength of concrete. All lightweight and natural normal weight aggregates were batched in a damp state and a saturated surface dried state, respectively. The amount of water absorbed in lightweight aggregates was accounted for in the mixture-proportioning procedure.

Control specimens of 150×300 mm cylinder were cast and cured simultaneously with the beam specimens in order to determine the compressive strength f'_c and splitting tensile strength f_{sp} of concrete. The results of compressive and splitting tensile strengths of concrete obtained from testing

of three cylinders at the same time as each beam test are given in Table 1. The air content of fresh concrete and dry density of hardened concrete are also presented in Table 1. The average ratios of f_{sp} to $\sqrt{f'_c}$ for ALWC, SLWC and NWC are 0.47, 0.53 and 0.59, respectively, nearly independent of the maximum aggregate size.

Test set-up

All deep beams having two spans were tested to failure under a symmetrical two-point top loading system with a vertical displacement rate of 0.3 mm/min using a 3000 kN capacity universal testing machine, as shown in Fig. 2. The two exterior end supports were designed to allow horizontal and rotational movements, whereas the intermediate support allowed only rotation. In order to evaluate the shear force and load distribution at supports, two load cells of a 1000 kN capacity and a load cell of 2000 kN capacity were located at both exterior end supports and intermediate support, respectively. Steel plats of different widths were provided at support and loading points, as shown in Fig. 2. Each beam was preloaded up to a total load of 150 kN before testing in order to assure a similar support reaction distribution to the result of a linear two-dimensional finite element (2-D FE) analysis.

Vertical deflections of beam specimens were measured using 100 mm range linear variable differential transformers (LVDTs) at each mid-span and a distance of $0.45L$ from the center of exterior supports where the maximum deflection is predicted to occur using a linear 2-D FE analysis. Both surfaces of all beams tested were whitewashed and gridded into a 100 mm square to aid on the observation of the occurrence and propagation of cracks during testing. The diagonal crack width of concrete struts joining the edges of loading and support plates was monitored by the PI type gages. Strains in longitudinal top reinforcement were also measured by 5 mm electrical resistance strain

(ERS) gages at the region crossing the line joining the edges of loading and intermediate support plates. All test data were captured by a data logger and automatically stored.

TEST RESULTS AND DISCUSSIONS

Crack propagation and failure mode

Figure 3 shows typical crack propagation in five test specimens having maximum aggregate size d_a of 4 mm or 19 mm at different load levels. The crack propagation after peak load is plotted using a '+' mark line type. The first diagonal crack developed suddenly at the mid-depth of the concrete strut within interior shear spans. The ratio of the first diagonal crack load within the interior shear span to the load capacity of the deep beams tested ranged between 0.51 and 0.70, as listed in Table 3; this ratio generally decreased with the increase of the maximum aggregate size and a lower ratio was exhibited by NWC deep beams than by lightweight concrete (LWC) deep beams. This indicates that the reserve strength, which is commonly defined as the retained strength after the occurrence of the first diagonal crack to the peak strength [13], can be enhanced with the increase of the size and strength of coarse aggregate. On the other hand, most of the beams tested showed no flexural vertical cracks in the sagging or hogging region until failure as the shear span-to-overall depth ratio a/h is very small. As the load increased, more diagonal cracks were formed within the interior and exterior shear spans until failure occurred due to a significant diagonal crack connecting the edges of the loading and intermediate support plates. All specimens failed in diagonal shear prior to reaching their flexural capacity. Although, all beams failed un-symmetrically and cracks after the peak load developed densely in the failed span, nearly the same crack patterns were observed in both spans up to the peak load. At the peak load, the increase of aggregate size led to more diagonal cracks. After the peak load, new diagonal cracks also developed within the interior and the exterior shear spans.

Load versus mid-span deflection

It was observed that the beam deflection measured at mid-span became slightly larger than that measured at $0.45L$ from the exterior support after the occurrence of the first diagonal crack within the interior shear spans. Therefore, the mid-span deflections of the failed span of different beams tested against the total applied load are only plotted in Fig. 4. The initial stiffness of beams tested was independent of the aggregate size and type of concrete. However, the stiffness after the occurrence of diagonal cracks within the interior shear spans gradually reduced with the increase of the applied load. The gradual stiffness reduction was more prominent in LWC deep beams than in NWC deep beams and increased with the decrease of the maximum aggregate size. Overall, the deflection of beams tested at the peak load generally decreased with the increase of the maximum aggregate size.

Support reactions

Figure 5 plots the end and intermediate support reactions against the total applied load. On the same figure, the support reactions obtained from a 2D linear FE analysis are also presented for a deep beam having similar properties to beams with 19 mm maximum aggregate size. The measured support reactions of all beam specimens were in agreement with those predicted from the 2D linear FE analysis until the occurrence of the first diagonal crack within the interior shear spans. However, the intermediate support reaction became slightly lower than FE predictions after the occurrence of diagonal cracks within the interior shear span due to stiffness reduction. The redistribution of the applied load after the occurrence of the first diagonal crack within the interior shear spans was slightly influenced by the aggregate size and the type of concrete. The measured intermediate support reactions of beams at peak load were lower than FE predictions by an average of 10.3% for ALWC beams, 10.2% for SLWC beams, and 5.3% for NWC beams, showing that a larger redistribution of loads occurred in LWC deep beams. The ratio, β_i , of the intermediate support

reaction to the total applied load at the ultimate strength of the beams tested increased with the increase of aggregate size; a slightly higher ratio was shown by NWC beams than LWC beams, as given in Table 3. A closer inspection of the failure surface of beams tested revealed that the failure surface of NWC beams is rougher than that of LWC beams and the surface roughness increases with the increase of the maximum aggregate size. As a result, the smoother failure surface, i.e. less aggregate interlock, reduces the load transfer capacity along the diagonal cracks and consequently causes a smaller β_1 .

Diagonal crack width

The width development of diagonal cracks along the diagonal plane joining the edges of loading and intermediate support plates is plotted against the total applied load in Fig. 6. The diagonal crack width was significantly influenced by the size and strength of coarse aggregates. Soon after the occurrence of the first diagonal crack, the diagonal crack width of beams of maximum aggregate size d_a of 4 mm sharply increased compared with that of beams having d_a above 8 mm. The increasing rate of diagonal crack width for concrete beams against the total applied load decreased with the increase of the maximum aggregate size, regardless of the type of concrete. At the same load level, the smallest diagonal crack width was recorded for NWC deep beams. Overall, the wider diagonal crack width within the interior shear spans, the less load transferred to the intermediate support, as depicted in Figs. 5 and 6. After the peak load, the diagonal crack width dramatically increased; however the increasing rate was more prominent in ALWC deep beams than in NWC deep beams.

Strains in main longitudinal reinforcement

Figure 7 shows the strains recorded in the main longitudinal top reinforcing bars at the region crossing the line between the edges of loading and intermediate support plates in beams having maximum aggregate size d_a of 4 mm or 19 mm. The longitudinal top reinforcement at loading points experienced compressive strains before the occurrence of the first diagonal crack within the

interior shear spans. However, the strains in top steel bars dramatically changed to tensile strains with the occurrence of the first diagonal cracks, showing that the increasing rate of the strain due to the tie action against the applied load was nearly independent of the type of concrete. At peak load, the tensile strains in longitudinal reinforcement of beams having d_a of 4 mm were much lower than that in beams having d_a of 19 mm. This indicates that the increase of load capacity of beams due to the enhanced aggregate interlock can produce a higher load transfer by tie action. No longitudinal reinforcement of the beam specimens reached its yield strain until the beam failure.

Load capacity of beams tested

The normalized diagonal cracking load within the interior shear spans, $\eta_{cr} = \frac{(P_{cr})_I}{bh\sqrt{f'_c}}$, was little influenced by the maximum aggregate size, as presented in Table 3. However, a slightly higher η_{cr} was observed in NWC deep beams than in LWC deep beams. This may be attributed to the fact that the splitting tensile strength of NWC was higher than that of LWC, as given in Table 1. However, the normalized load capacity, $\eta_n = \frac{P_n}{bh\sqrt{f'_c}}$, of beams tested increased with the increase of aggregate size, indicating that η_n for ALWC deep beams was lower than that for SLWC deep beams, which in turn was also lower than that for NWC deep beams, as shown in Fig. 8. In addition, the normalized load capacity of beams having d_a of 4 mm was much lower than that of beams having d_a above 8 mm, regardless of the type of concrete. The increasing rate for η_n against the maximum aggregate size was lower in LWC deep beams than in NWC deep beams, while a similar increasing rate was observed in both ALWC and SLWC deep beams. The normalized load capacity of beams with d_a of 19 mm was higher than that of beams with d_a of 4 mm by 140%, 135% and 156% for ALWC, SLWC, and NWC deep beams, respectively. A closer inspection of the failure surface of the beams

tested revealed that the failure surface of NWC is formed along the cement paste round the aggregate particles, while that in LWC beams is mainly formed through coarse aggregate particles, though some un-splitting aggregate particles are also detected. Therefore, the increase of aggregate size caused a rougher failure surface that allows higher shear stresses to be transferred along diagonal cracks in NWC than LWC deep beams; though the larger aggregate size used in LWC beams, the higher load capacity achieved.

STRUT-AND-TIE MODELS FOR CONTINUOUS DEEP BEAMS

Figure 9 shows a schematic strut-and-tie model for continuous deep beams subjected to two-point symmetrical top loads in accordance with ACI 318-08 [1] and EC 2 [2]. There are two main load transfer systems, one of which is the strut-and-tie action associated with the longitudinal bottom reinforcement acting as a tie in sagging zones and the other is the strut-and-tie action due to the longitudinal top reinforcement in the hogging zone. As the applied loads in the two-span continuous deep beams are directly transferred to supports through concrete struts of exterior and interior shear spans, the load capacity of two-span continuous deep beams, P_n , owing to failure of concrete struts is

$$P_n = 2(F_E + F_I) \sin \theta \quad (1)$$

where F_E and F_I = load capacities of exterior and interior concrete struts, respectively, and θ = angle of the concrete strut to the longitudinal axis of the deep beam, which can be expressed as $\tan^{-1}(jd/a)$, where a = shear span and jd = distance between the centers of the top and bottom nodes. ACI 318-08 specifies that θ shall not be less than 25° . On the other hand, EC 2 recommends that $1 \leq \theta \leq 2.5$. From the geometrical dimension, jd can be assumed as follows:

$$jd = h - (w_t + w_t')/2 \quad (2)$$

where h = overall section depth, and w_t and w_t' = depths of bottom and top nodes, respectively. ACI 318-08 [1] recommend that the depth of the bottom node can be approximately assumed as the lesser of the height of the plate anchored to the bottom longitudinal reinforcement and twice the concrete cover ($= 2c$) of the longitudinal reinforcement, as shown in Fig. 9. The depth of the top node w_t' can be determined from the equilibrium of forces of the limit of resultant compressive force, C , in the top node and the limit of resultant tensile force in the bottom node [14]. The limit of resultant compressive and tensile forces can be obtained based on the concrete effective stresses in the nodal zones. From the effective stress of the nodal zones specified in the code provisions, the depth of the top node, w_t' , can be expressed as $0.8w_t$ for ACI 318-08, and $0.85w_t$ for EC 2.

As the nodes at the applied load point can be classified as a CCC type that has equal stresses on all in-plane sides, the ratio of each face width of the hydrostatic node has to be the same as the ratio of the forces meeting at the node to make the state of stress in the node region constant [3, 14]. Therefore, the width of each loading plate can be approximately subdivided into two parts in accordance with the ratio, β_t , of the intermediate support reaction to the applied load. The load transferred to the intermediate support slightly decreased in comparison with that predicted by a linear finite element (FE) analysis after the occurrence of the first diagonal crack within the interior shear spans, but this difference is generally less than 5~10% for concrete beams, as shown in Fig. 5. Therefore, the value of β_t can be estimated from a linear finite element (FE) analysis considering shear deformation. The effective strut width is dependent on the width of the tie and loading plate, and the slope of the strut. The average effective widths of concrete struts uniformly tapered in interior, $(w_s)_I$, and exterior shear spans, $(w_s)_E$, can be calculated from:

$$(w_s)_I = \frac{(w_t + w_t') \cos \theta + [0.5(l_p)_I + \beta_t (l_p)_P] \sin \theta}{2} \quad (3-a)$$

$$(w_s)_E = \frac{(w_t + w'_t) \cos \theta + [(l_p)_E + (1 - \beta_t)(l_p)_P] \sin \theta}{2} \quad (3-b)$$

where $(l_p)_P$, $(l_p)_E$ and $(l_p)_I$ = widths of loading, end support and intermediate support plates, respectively. The load transfer capacity of concrete struts depends on the strut area and effective concrete compressive strength. Hence, load capacities of exterior and interior concrete struts are

$$F_E = v_e f'_c b_w (w_s)_E \quad (4-a)$$

$$F_I = v_e f'_c b_w (w_s)_I \quad (4-b)$$

where v_e = effectiveness factor of concrete that is introduced to account for the limited ductility of concrete and various sources affecting the deterioration of concrete strength. For concrete struts without shear reinforcement, ACI 318-08 recommends an effectiveness factor of 0.6λ , whereas EC 2 gives it as $0.6\lambda(1 - f'_c/250)$, where λ = modification factor to account for the reduced friction properties and splitting tensile resistance of lightweight concrete compared with normal weight concrete of the same compressive strength. For beams where splitting tensile strength of concrete not measured, ACI 318-08 recommends that $\lambda = 0.75$ for ALWC, and 0.85 for SLWC. Linear interpolation can be used to obtain these factors according to the volumetric fractions of lightweight fine or coarse aggregates to normal weight fine or coarse aggregates, respectively. On the other hand, EC 2 classifies lightweight concrete according to its dry density and specifies λ as follows:

$$\lambda = 0.4 + 0.6\rho_u / 2200 \quad (5)$$

where ρ_u = the upper limit of the dry density for the relevant class. EC 2 classifies the design density of lightweight concrete at the spacing of 200 kg/m³ from 800 kg/m³ to 2000 kg/m³.

Comparisons of modification factors

In STM models specified in the code provisions, the effect of the type of concrete on the load transfer capacity of concrete struts is only accommodated in the modification factor of the effectiveness factor of concrete, as explained above. On the other hand, the corresponding

experimentally modification factor for lightweight concrete can be evaluated as the ratio of the load capacity of LWC deep beams to that of the companion NWC deep beams. Figure 10 shows the comparison of the modification factors measured from the present experimental results and proposed by the ACI 318-08 and EC 2 for lightweight concrete. The modification factor for LWC continuous deep beams tested slightly decreased with the increase of the maximum aggregate size. The modification factor specified in EC 2 is higher than that of ACI 318-08 for the beams tested. In addition, EC 2 generally overestimates the modification factor for ALWC continuous deep beams, indicating that the unconservatism increases with the increase of the maximum aggregate size. The modification factor specified in ACI 318-08 is generally conservative for ALWC deep beams, but unconservative for SLWC deep beams with aggregate size above 13 mm.

Comparisons of measured and predicted load capacities

The ratio, $\gamma_{cs} = (P_n)_{Exp.} / (P_n)_{Pre.}$, between measured and predicted by STM load capacities of the current deep beams is given in Table 3. The means of γ_{cs} obtained from the comparison of ACI 318-08 for ALWC, SLWC and NWC continuous deep beams are 1.307, 1.221 and 1.297, respectively, while those of EC 2 are 1.337, 1.329 and 1.468, respectively. The means of γ_{cs} for both code provisions are slightly lower for LWC deep beams than NWC deep beams. In addition, the ratio γ_{cs} generally decreased with the decrease of the maximum aggregate size, regardless of the type of concrete. The conservatism of STMs specified in both codes consequently decreases with the decrease of the size and strength of coarse aggregates.

CONCLUSIONS

Based on the test results and comparisons with ACI 318-08 and EC 2 provisions, the following conclusions may be drawn:

1. The formation of failure plane of beams tested was hardly influenced by the maximum aggregate size and the type of concrete.
2. The gradual stiffness reduction after the occurrence of diagonal cracks was more prominent in lightweight concrete deep beams than in normal weight concrete deep beams and increased with the decrease of the maximum aggregate size.
3. The ratio of the intermediate support reaction to the total applied load at peak load increased with the increase of maximum aggregate size, and was larger in normal weight concrete beams than in lightweight concrete beams.
4. The diagonal crack width decreased with the increase of the maximum aggregate size and was smaller in normal than lightweight concrete deep beams at the same load level.
5. The normalized diagonal cracking load within the interior shear spans of beams tested was little influenced by the maximum aggregate size. However, the normalized load capacity of beams tested increased with the increase of the maximum aggregate size. In addition, the normalized load capacity for all-lightweight concrete beams was lower than that for sand-lightweight concrete deep beams, which in turn was also lower than that for normal weight concrete deep beams having the same maximum aggregate size.
6. The ratio of the load capacity of lightweight concrete continuous beams to that of the companion normal weight concrete continuous beams commonly decreased with the increase of the maximum aggregate size.
7. The modification factor for lightweight concrete deep beams in EC 2 is generally unconservative, while that in ACI 318-08 is conservative for all-lightweight concrete but unconservative for sand-lightweight concrete with the maximum aggregate size above 13 mm.
8. The conservatism of the strut-and-tie models specified in ACI 318-08 and EC 2 decreased with the decrease of the maximum aggregate size, and was less in lightweight concrete deep beams than in normal weight concrete deep beams.

KNOWLEDGMENTS

This work was supported by the Korea Science and Engineering Foundation (KOSEF) grant funded by the Korea government (MEST) (R01-2008-000-20395-0), and the Grant of the Korean Ministry of Education, Science and Technology (The Regional Core Research Program/Biohousing Research Institute).

REFERENCES

- [1] ACI Committee 318. Building code requirements for structural concrete (ACI 318-08) and commentary (ACI 318R-08). American Concrete Institute 2008; Farmington Hills, MI: 473 pp.
- [2] The European Standard EN 1992-1-1:2004. Eurocode 2: design of concrete structures. British Standards Institution 2004; London, UK: 225 pp.
- [3] Marti P. Basic tools of reinforced concrete beam design. ACI Structural Journal 1985; 82(1): 46-56.
- [4] Taylor HPJ. Investigation of forces carried across cracks in reinforced concrete beams in shear by interlock of aggregate. TRA 42.447, Cement and Concrete Association 1970: 22 pp.
- [5] Fenwick RC, Paulay T. Mechanisms of shear resistance of concrete beams. Journal of the Structural Division, ASCE 1968; 94(10): 2235-2350.
- [6] Walraven J, Lehwalter N. Size effects in short beams loaded in shear. ACI Structural Journal 1994; 91(5): 585-593.

- [7] Bažant ZP, Sun HH. Size effect in diagonal shear failure: influence of aggregate size and stirrups. *ACI Materials Journal* 1987; 84(4): 259-272.
- [8] Collins MP, Kuchma D. How safe are our large, lightly reinforced concrete beams, slabs, and footings?. *ACI Structural Journal* 1999; 96(4): 482-490.
- [9] Sherwood EG, Bentz EC, Collins MP. Effect of aggregate size on beam-shear strength of thick slabs. *ACI Structural Journal* 2007; 104(2): 180-190.
- [10] Bentz EC, Vecchio FJ, Collins MP. Simplified modified compression field theory for calculating shear strength of reinforced concrete elements. *ACI Structural Journal* 2006; 103(4): 614-624.
- [11] Schlaich J, Schäfer K, Jennewein M. Toward a consistent design of structural concrete. *Journal of the Prestressed Concrete Institute* 1987; 32(3): 74-150.
- [12] Yang KH, Ashour AF. Code modeling of reinforced concrete deep beam. *Magazine of Concrete Research* 2008; 60(6): 441-454.
- [13] Tan KH, Kong FK, Weng LW. High-strength reinforced concrete deep and short beams: shear design equations in north American and UK Practice. *ACI Structural Journal* 1998; 95(3): 318-329.
- [14] Yang KH, Ashour AF. Load capacity of reinforced concrete continuous deep beams. *Journal of Structural Engineering, ASCE* 2008; 134(6): 919-929.

TABLES AND FIGURES

List of Tables:

Table 1 – Details of test specimens and mix proportions.

Table 2 – Physical properties of aggregates used.

Table 3 – Summary of test results and comparisons with STM predictions.

List of Figures:

Fig. 1 – Details of beam geometry and arrangement of reinforcements.

Fig. 2 – Test setup.

Fig. 3 – Typical crack patterns and failure modes.

Fig. 4 – Total load versus mid-span deflection.

Fig. 5 – Support reactions against total load.

Fig. 6 – Diagonal crack width against total load.

Fig. 7 – Strains in main longitudinal top reinforcement.

Fig. 8 – Effect of aggregate size on the normalized load capacity.

Fig. 9 – Schematic strut-and-tie model for continuous deep beams.

Fig. 10 – Comparisons of lightweight concrete modification factor in code provisions and experimental results.

Table 1-Details of test specimens and mix proportions

Specimen	Type of concrete	a_g (mm)	W/B	S/A	Unit weight [#] (kg/m ³)					R_{sp} (%)	f'_c (MPa)	f_{sp} (MPa)	ρ (kg/m ³)	A_c (%)
					W	C	SF	F	G					
A4	All-lightweight	4	0.4	-	139	348	0	1043	0	0.75	31.2	2.54	1510	6.4
A8		8	0.36	0.4	222	548	61	320	439	0.21	29.0	2.53	1540	5.8
A13		13	0.35		212	545	61	327	448	0.45	31.8	2.73	1551	5.2
A19		19	0.30		173	518	58	326	447	0.50	31.4	2.62	1514	4.9
S4	Sand-lightweight	4	0.52	-	260	495	0	1486*	0	0.00	34.8	3.35	2130	6.6
S8		8	0.35	0.4	198	569		634*	474	0.19	29.9	2.84	1841	5.2
S13		13	0.36		203	556		633*	473	0.15	34.0	3.10	1824	6.2
S19		19	0.33		171	525		625*	467	0.21	35.0	2.98	1772	5.0
N4	Normal-weight	4	0.50	-	250	502		1505*	0	0.00	25.8	2.89	2157	5.4
N8		8	0.65	0.4	201	309		715*	1097*	0.20	29.6	3.18	2233	4.4
N13		13	0.63		193	309		723*	1110*	0.13	27.4	3.09	2253	3.1
N19		19	0.60		186	309		731*	1122*	0.13	33.2	3.51	2273	2.9

Note : a_g = maximum size of aggregate, W/B = water-to-binder ratio by weight, S/A = fine aggregate-to-total aggregate ratio by volume, R_{sp} = ratio of superplasticizer to binder by weight, f'_c = compressive strength of concrete, f_{sp} = splitting tensile strength of concrete, ρ = dry density of hardened concrete, and A_c = air content.

W , C , SF , F , and G refer to water, ordinary portland cement, silica fume, fine aggregate, and coarse aggregate, respectively.

* indicates natural normal weight aggregates.

Table 2-Physical properties of aggregates used.

Type		Maximum size (mm)	Unit volume weight (kg/m ³)	Specific gravity	Water Absorption (%)	Porosity (%)	Fineness
Coarse aggregate	Expanded clay granule	19	709	1.04	20	68.17	6.68
		13	692	1.02	23	67.84	6.20
		8	727	1.07	19	67.91	5.55
	Andesite	19	1325	2.62	0.98	50.57	5.68
		13	1302	2.61	1.02	49.89	5.90
		8	1353	2.62	1.11	51.65	5.90
Fine aggregate	Expanded clay granule	4	832	1.65	28	50.42	2.43
	Sand	4	1637	2.51	1.58	65.21	2.32

Table 3–Summary of test results and comparisons with STM predictions

Specimen	Inclined cracking load (P_{cr}) and shear force (V_{cr}), (kN)				Load capacity (P_n) and corresponding shear strength (V_n) at failed span, (kN)			$\frac{(P_{cr})_I}{P_n}$	η_{cr}	η_n	β_t	Predicted P_n (kN)		$\frac{(P_n)_{Exp.}}{(P_n)_{Pre.}}$	
	Interior shear span		Exterior shear span		P_n	$(V_n)_I$	$(V_n)_E$					ACI 318-08	EC 2	ACI 318-08	EC 2
	$(P_{cr})_I$	$(V_{cr})_I$	$(P_{cr})_E$	$(V_{cr})_E$											
A4	594.7	161.7	577.5	147.5	847.3	215.3	208.3	0.70	1.332	1.897	0.508	821.9	802.2	1.031	1.056
A8	657.0	185.3	702.1	166.3	987.6	254.6	239.2	0.67	1.525	2.292	0.516	764.0	753.1	1.293	1.311
A13	729.6	210.4	887.8	192.2	1227.4	331.8	281.9	0.59	1.616	2.719	0.541	837.8	815.4	1.465	1.505
A19	712.4	205.0	841.7	195.5	1190.3	338.1	257.1	0.60	1.590	2.656	0.568	827.2	806.6	1.439	1.476
S4	712.5	202.9	796.0	163.9	1011.5	257.4	248.4	0.70	1.510	2.143	0.509	1039.0	994.8	0.974	1.017
S8	716.2	202.0	899.4	220.0	1209.4	315.6	289.1	0.59	1.637	2.764	0.522	892.7	823.8	1.355	1.468
S13	759.4	215.7	891.5	203.0	1267.1	354.3	279.3	0.60	1.628	2.717	0.559	1015.1	919.3	1.248	1.378
S19	759.8	222.5	1119.2	265.0	1367.8	372.0	311.9	0.56	1.605	2.890	0.544	1045.0	942.0	1.309	1.452
N4	651.3	182.5	760.8	190.3	929.3	236.7	227.9	0.70	1.603	2.287	0.509	906.2	812.7	1.025	1.143
N8	790.3	229.8	1020.8	226.8	1277.0	365.2	273.3	0.62	1.817	2.936	0.572	1039.7	916.6	1.228	1.393
N13	805.0	234.9	1259.5	305.1	1466.6	421.8	311.5	0.55	1.923	3.503	0.575	962.5	857.0	1.524	1.711
N19	840.8	240.0	1348.9	301.5	1643.4	489.2	332.5	0.51	1.824	3.565	0.595	1166.2	1011.3	1.409	1.625

Note] Interior and exterior shear spans are identified by subscripts I and E , respectively.

$$\eta_{cr} \left(= \frac{(P_{cr})_I}{bh\sqrt{f'_c}} \right) = \text{normalized inclined cracking load, } \eta_n \left(= \frac{P_n}{bh\sqrt{f'_c}} \right) = \text{normalized load capacity, and } \beta_t = \text{ratio of the intermediate support reaction to}$$

the total applied load at the ultimate strength of beams tested.

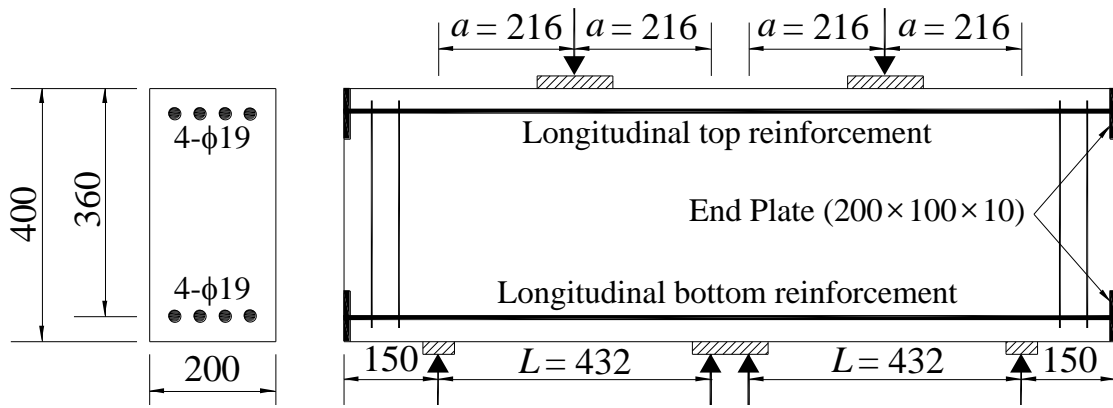


Fig. 1-Details of beam geometry and arrangement of reinforcement
(All dimensions are in mm).

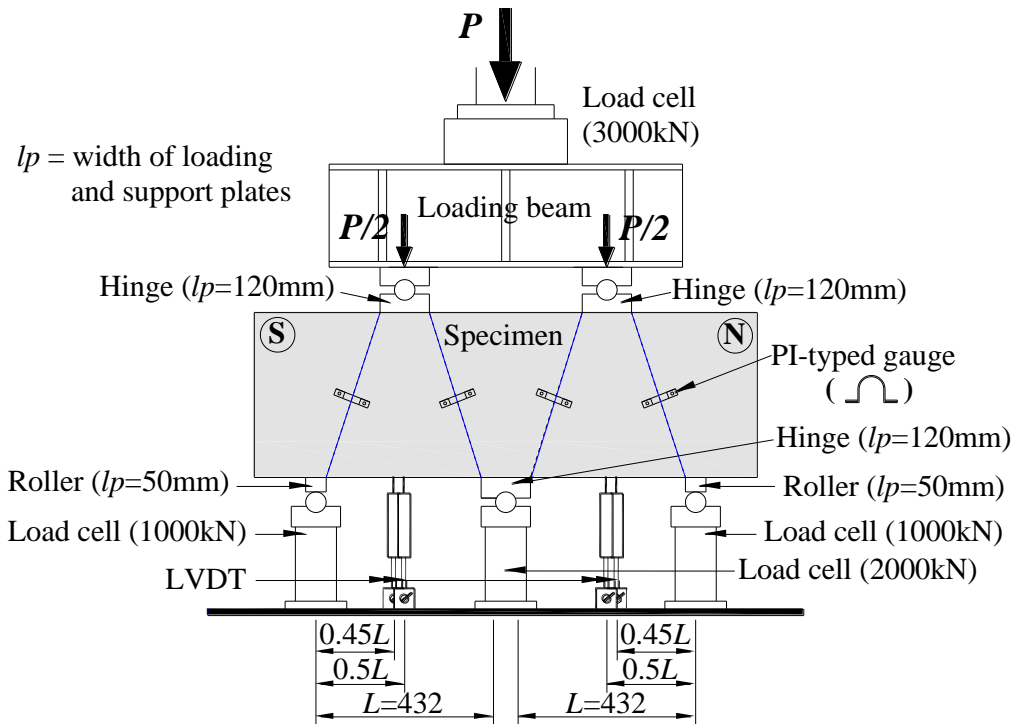
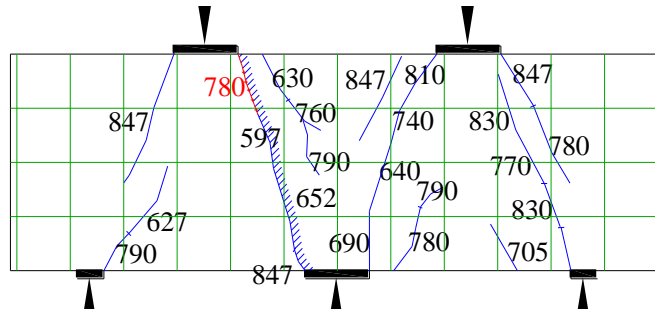
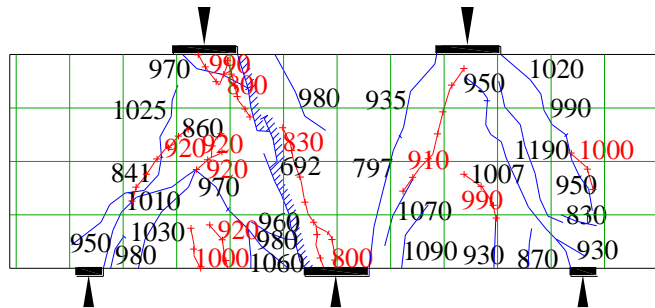


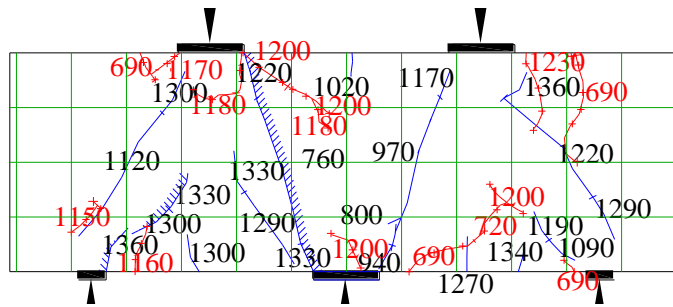
Fig. 2-Test setup.



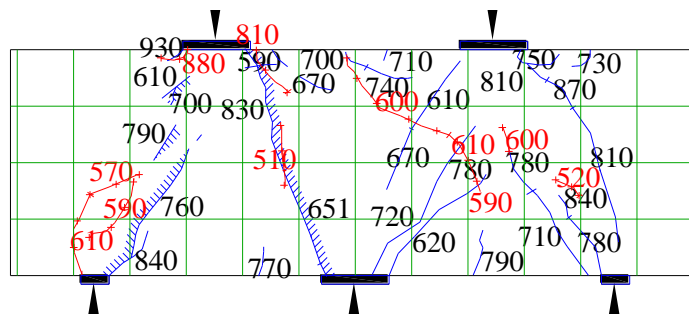
(a) Specimen A-4 (all-lightweight concrete with $d_a = 4\text{mm}$)



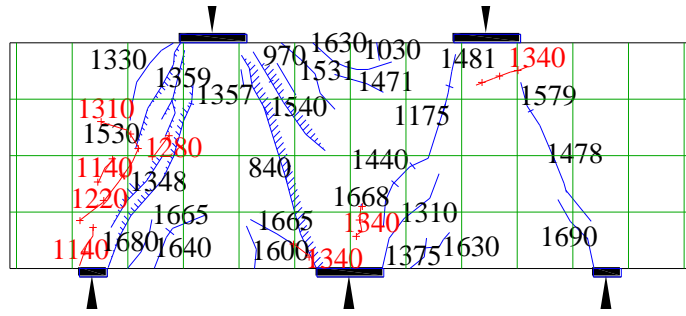
(b) Specimen A-19 (all-lightweight concrete with $d_a = 19\text{ mm}$)



(c) Specimen S-19 (sand-lightweight concrete with $d_a = 19\text{ mm}$)



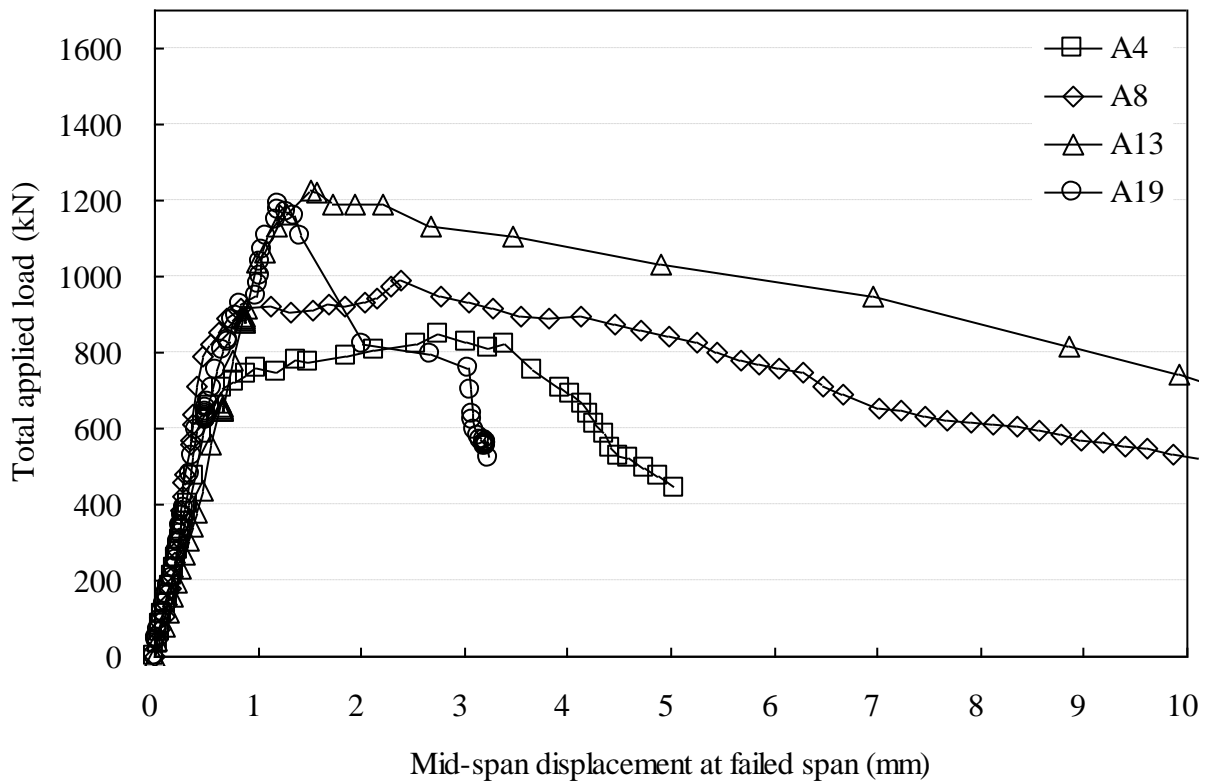
(d) Specimen N-4 (normal weight concrete with $d_a = 4\text{mm}$)



(e) Specimen N-19 (normal weight concrete with $d_a=19$ mm)

Fig. 3-Typical crack patterns and failure modes.

(Numbers indicate the total load in kN at which a crack occurred, and cross-hatchings indicate the failure zone of concrete. Crack propagation after peak load is also plotted using a “+” mark)



(a) ALWC deep beams

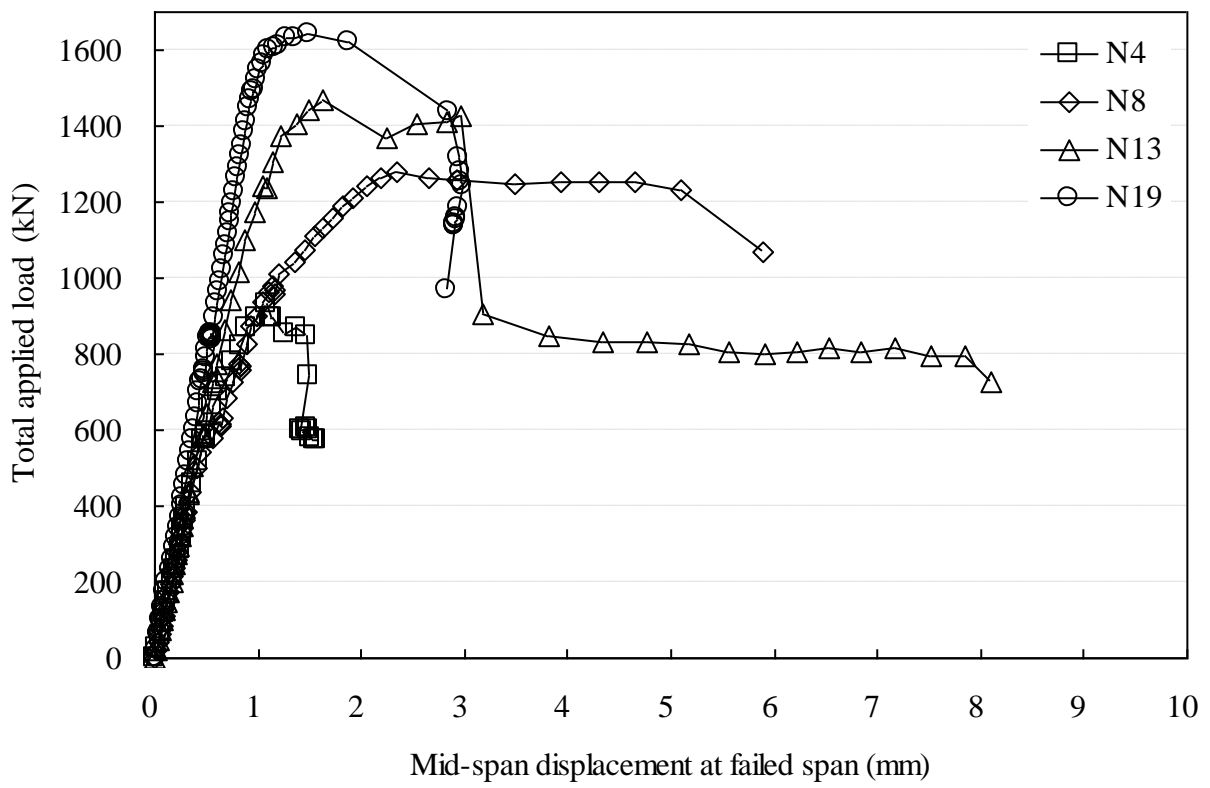
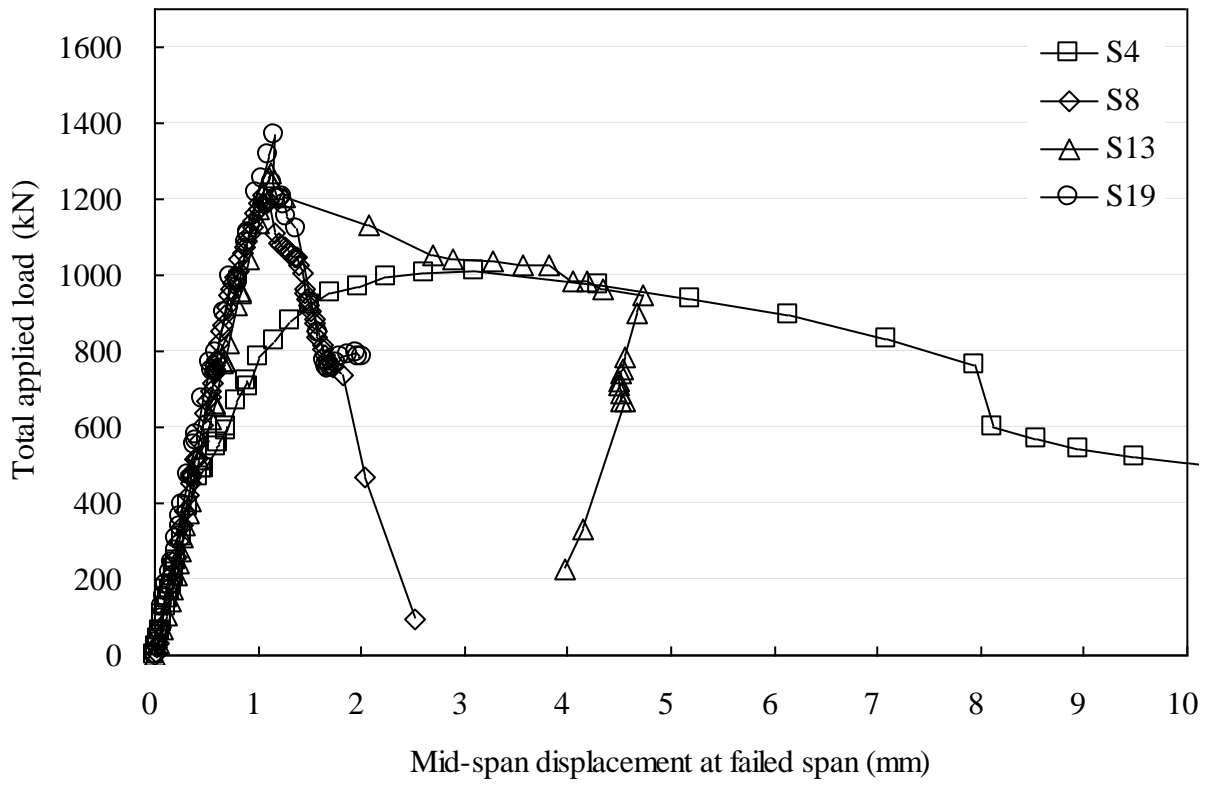
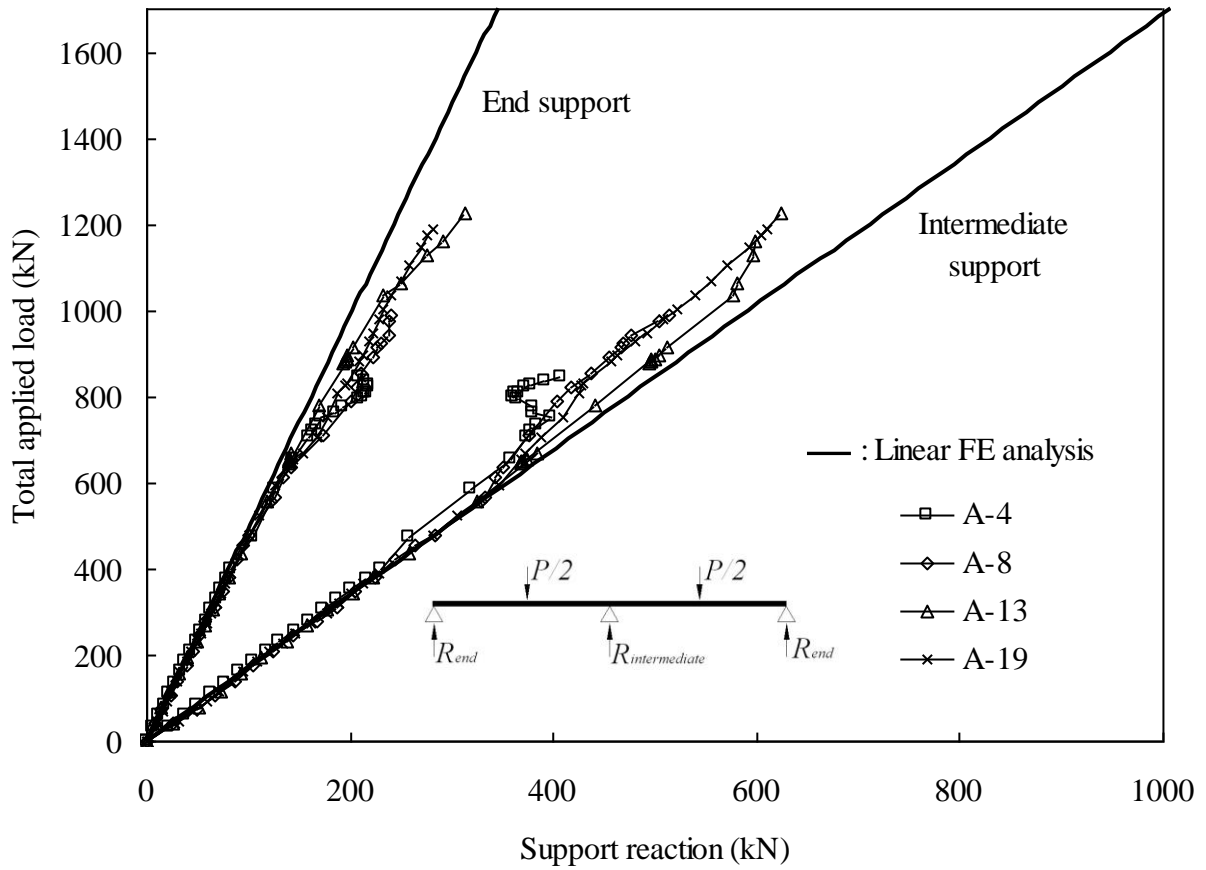
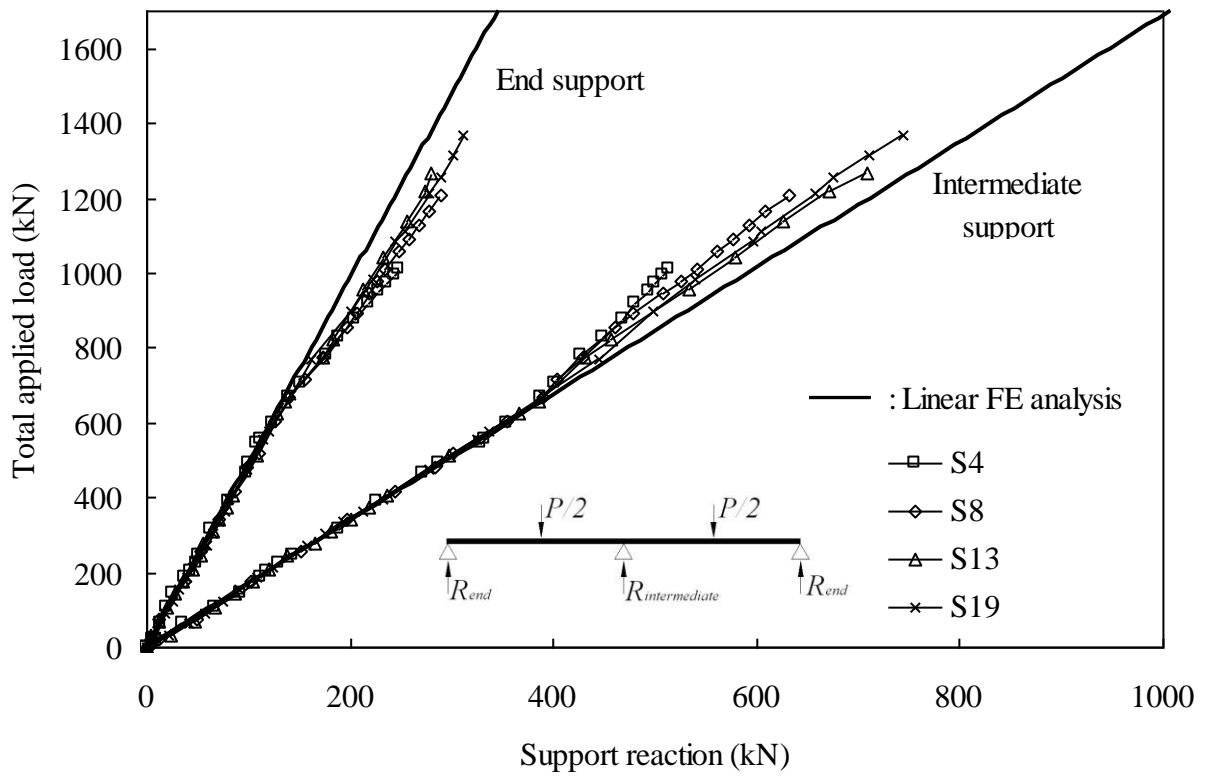


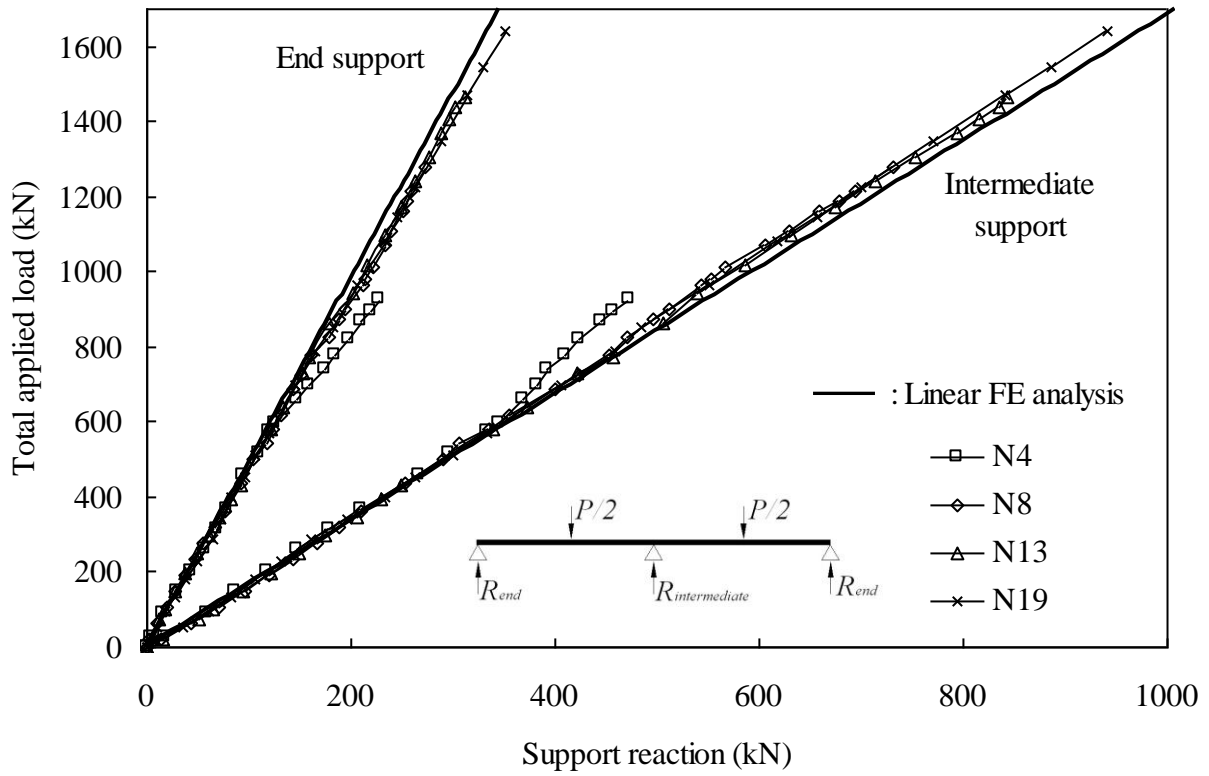
Fig. 4-Total load versus mid-span deflection.



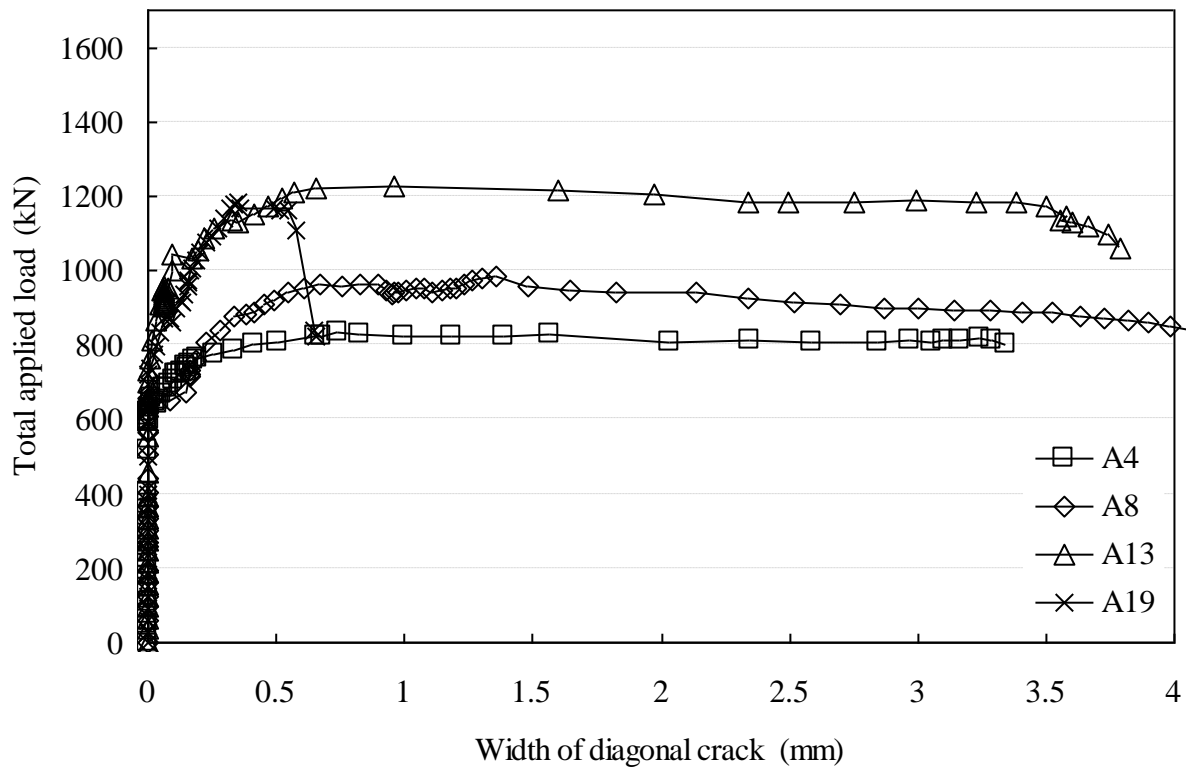
(a) ALWC deep beams



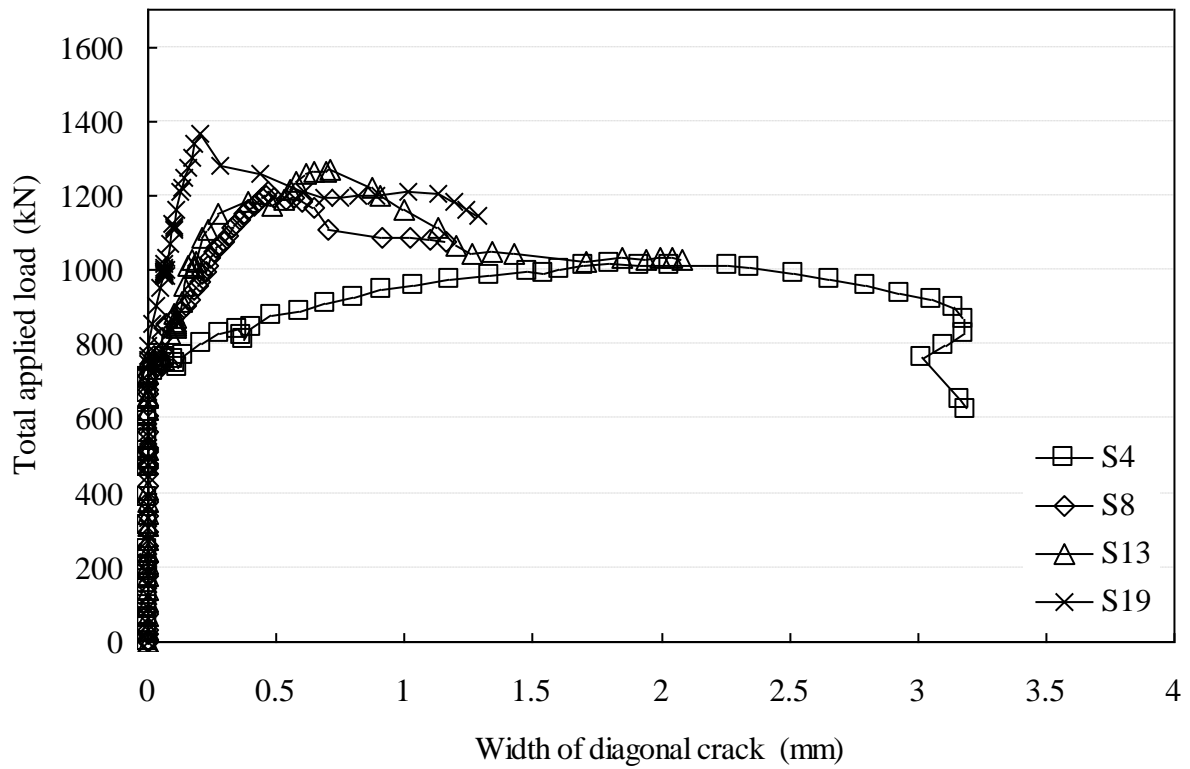
(b) SLWC deep beams



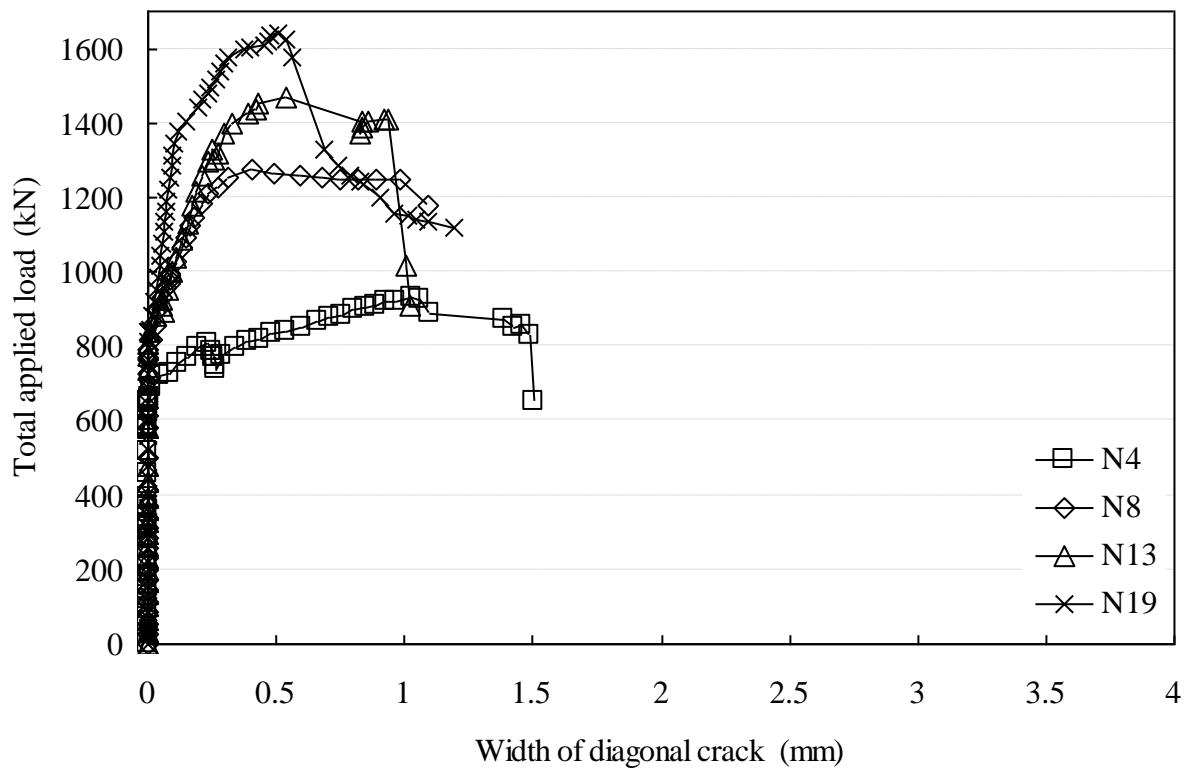
(c) NWC deep beams
Fig. 5-Support reactions against total load.



(a) ALWC deep beams



(b) SLWC deep beams



(c) NWC deep beams

Fig. 6-Diagonal crack width against total load.

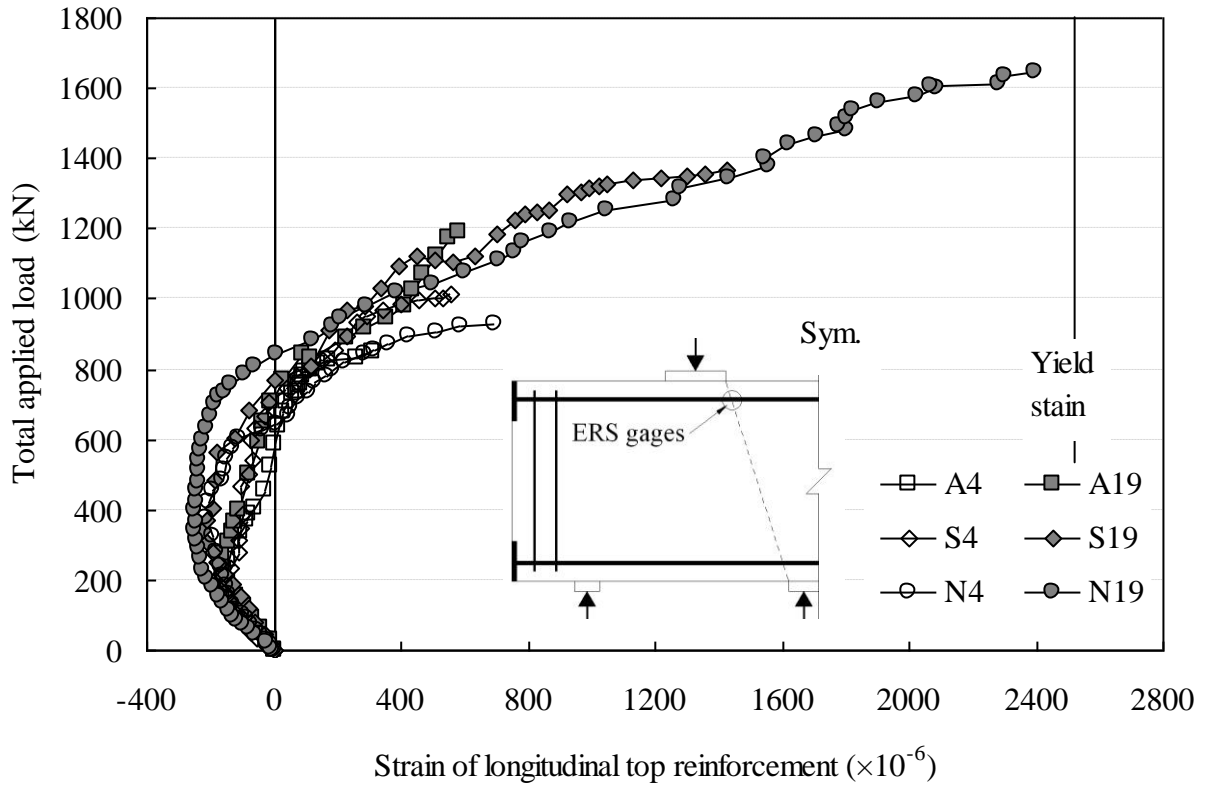


Fig. 7-Strains in main longitudinal top reinforcement.

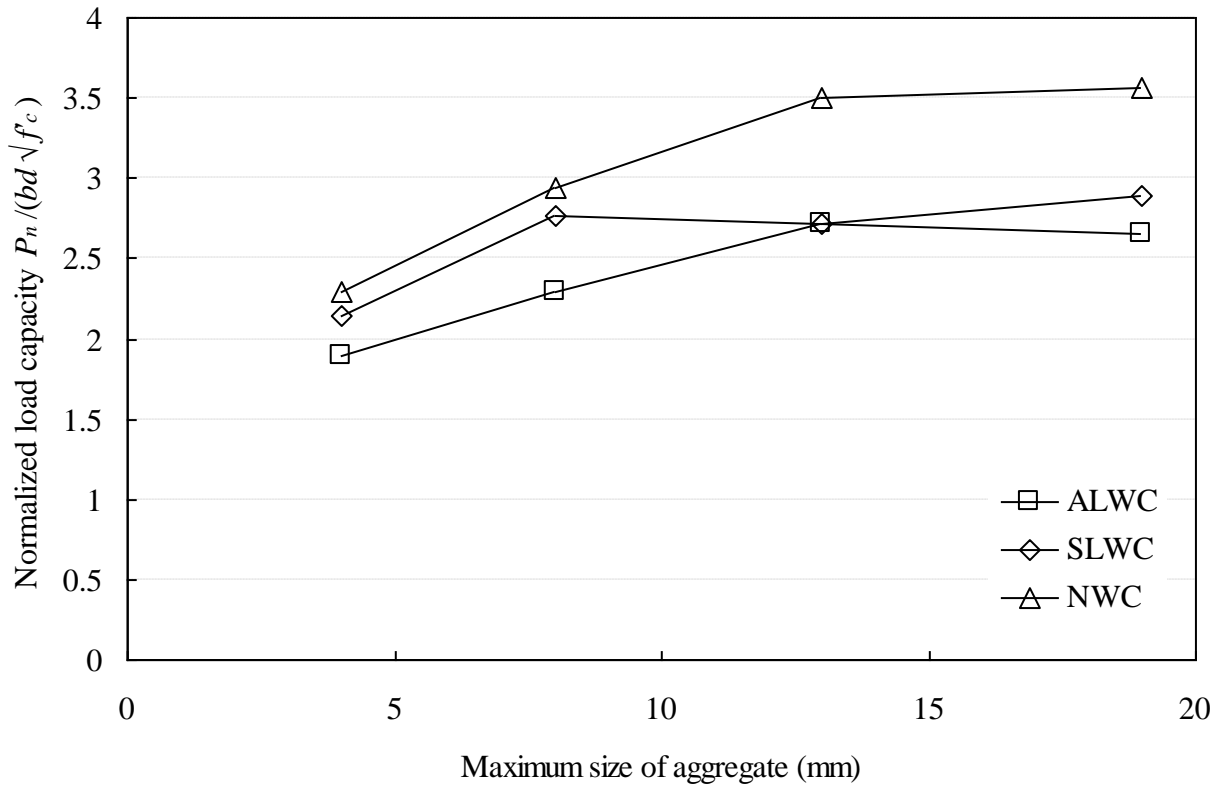


Fig. 8-Effect of aggregate size on the normalized load capacity.

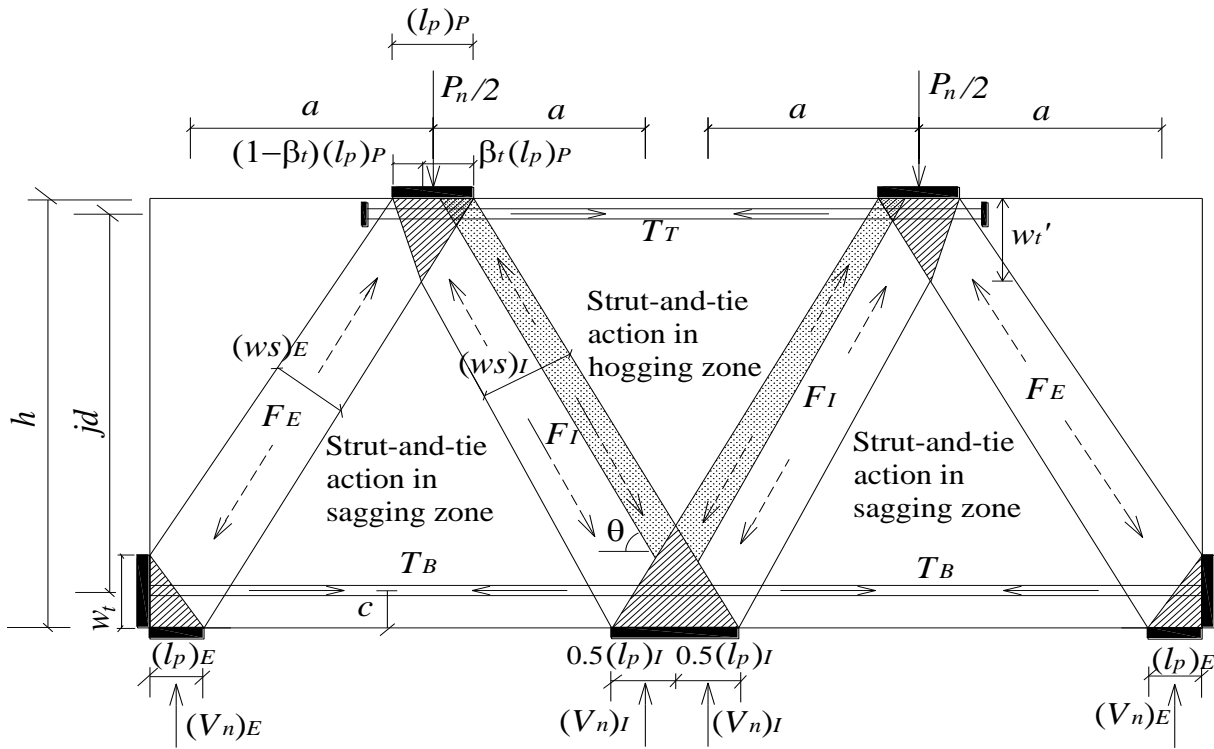


Fig. 9-Schematic strut-and-tie model for continuous deep beams.

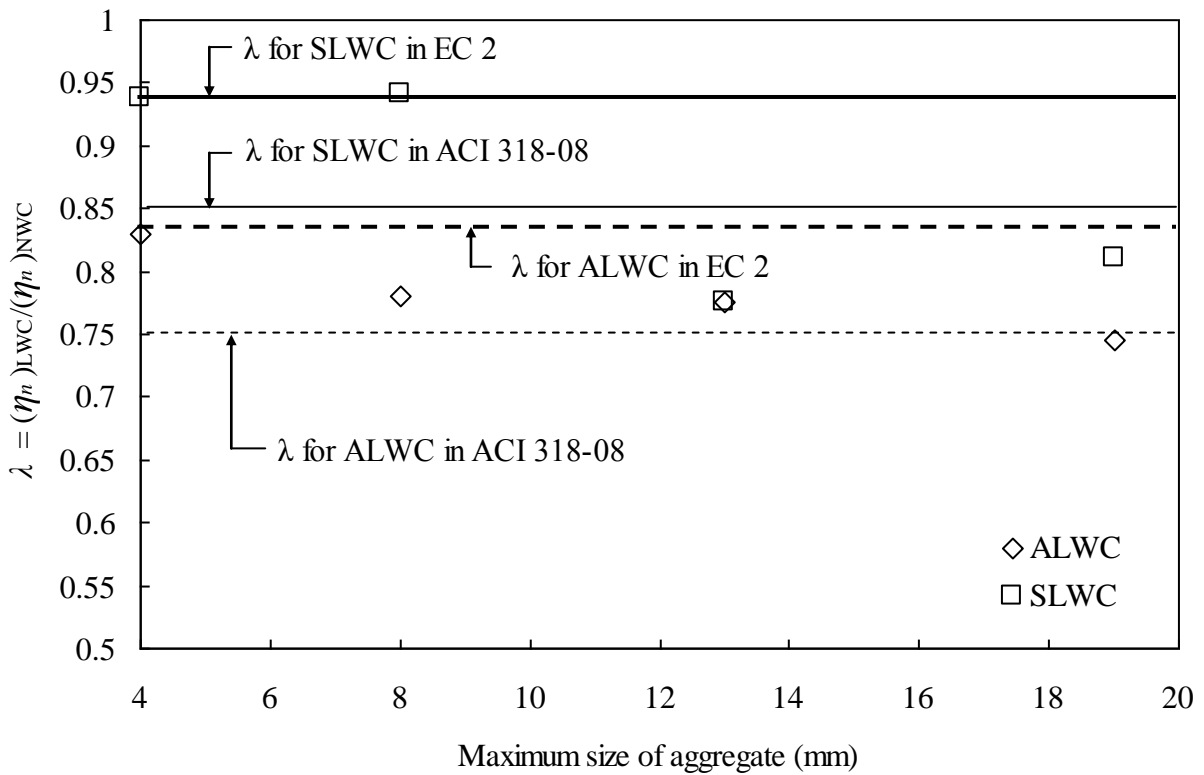


Fig. 10-Comparisons of lightweight concrete modification factor in code provisions and experimental results.